2025 American Control Conference (ACC)
July 8-10, 2025. Denver, CO, USA

Fault Diagnosis of Electrolyte Lithium Concentration in Lithium-ion Batteries

Sara Sepasiahooyi and Shu-Xia Tang

Abstract— **Faults in lithium-ion batteries can diminish performance and shorten lifespan. One notable electrochemical fault arises from the loss of lithium concentration in the electrolyte, which can lead to degradation over time. This paper studies the detection and estimation of electrolyte lithium concentration degradation fault in battery cells. The proposed model-based fault detection scheme consists of two cascaded closed-loop Partial Differential Equation (PDE) observers. The first observer, state observer, estimates the distributed lithium concentration in the electrolyte. The second observer, fault estimator, utilizes the concentration estimated by the first observer to detect and estimate the electrolyte lithium concentration fault. The scheme is validated through simulations conducted on a $LiFePO_4$ battery cell under an Urban Dynamometer Driving Schedule (UDDS) current profile.**

Index Terms— **Lithium-ion battery; Degradation; Electrolyte; Fault detection; Fault estimation.**

I. Introduction

Faults in lithium-ion batteries can arise due to electrochemical, thermal, or mechanical factors, potentially affecting performance, safety, and longevity [1]. One of the significant factors contributing to the aging of lithium-ion batteries is the loss of electrolytes [2]. High cell voltage and elevated temperatures can cause electrolyte decomposition, leading to a loss of lithium inventory and eventual capacity fade. In addition, at low temperatures, lithium plating significantly contributes to performance degradation, including loss of lithium inventory [3]. This paper studies electrolyte lithium concentration faults, which occur due to electrolyte loss in the battery. This fault will be caused by battery degradation mechanism such as Solid Electrolyte Interphase (SEI) growth [4]. Identifying electrolyte faults is beneficial for diagnosing battery health. Equivalent circuit models are effective for identifying electrical faults such as short circuits [5]. However, they cannot effectively detect electrochemical faults. Electrochemical battery models provide representation of lithium concentration dynamics and are suited for identifying such faults.

In [6], electrode-level faults are detected by reformulating the PDEs of the Single Particle Model (SPM) into Ordinary Differential Equations (ODEs) and designing an ODE observer. Ferdowsi et al. in [7] worked on solid-phase lithium concentration faults, through the design of PDE observers and subsequently estimating the remaining useful life of the battery. In [8], electrochemical faults, including a decrease in diffusion coefficient, changes in particle size and porosity, and electrical contact loss, are detected, isolated, and estimated. In [9], two cascaded observers are employed to detect and estimate the distributed temperature fault of a battery cell.

In this study, we focus on detecting and estimating distributed electrolyte lithium concentration fault by designing two cascaded PDE observers: state observer for estimating the distributed electrolyte lithium concentration and the fault estimator for electrolyte fault diagnosis. The main contributions of this work are as follows:

- To the best of the authors' knowledge, this is the first time a model-based electrolyte-level fault detection and estimation scheme has been studied.
- The state estimation error for the observer estimating the system's state is assumed to be zero in Assumption 2 of [9], where our paper relaxes this assumption and explicitly accounts for estimation error.
- In [9], the fault is represented as a mathematically oriented function, whereas in this paper, an electrolyte fault expression with physically meaningful relevance is proposed.
- Compared to fault model in [7], which focuses on solid-phase lithium concentration degradation faults, we extend the electrolyte-phase lithium concentration degradation fault model by incorporating additional physically relevant terms.

In the rest of this paper, the nominal (fault-free) battery model is presented in Section II. In Section III, the system integrated with the fault is introduced, followed by the proposed fault function. The fault detection scheme is detailed in Section IV, with simulation results provided in Section V. Finally, Section VI presents the conclusion and future work.

II. System model

In this section, the electrolyte lithium concentration PDEs in the nominal battery model are presented. The schematic of the Single Particle Model with electrolyte (SPMe) dynamics is shown in Fig. 1. The current $I(\bar{t})$ and terminal voltage $V(\bar{t})$ are the system's input and output, respectively. $\bar{t}$ and $\bar{x}$ are the temporal and spatial coordinates, respectively. In this paper, the following assumption is considered:

Assumption 1. *Electrolyte effective diffusion coefficient,* $D_e^{i,eff}(c_e^i(\bar{t},\bar{x})), i \in \{-, sep, +\}$*, remains constant.*

The electrolyte lithium concentration in the positive and negative electrode $c_e^{\pm}(\bar{t},\bar{x})$, and modified boundary condi-

S. Sepasiahooyi and S.-X. Tang (Corresponding author) are with the Department of Mechanical Engineering, Texas Tech University, Lubbock, USA. ssepasia@ttu.edu, shuxia.tang@ttu.edu.

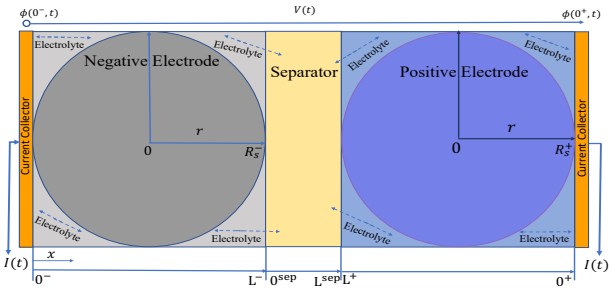

Fig. 1: Schematic of SPMe

tions [10] are described as:

$$\frac{\partial c_{\mathrm{e}}^{\pm}}{\partial \bar{t}}(\bar{t},\bar{x}) = \frac{D_{\mathrm{e}}^{\pm,\mathrm{eff}}}{\varepsilon_{\mathrm{e}}^{\pm}}\frac{\partial^2 c_{\mathrm{e}}^{\pm}(\bar{t},\bar{x})}{\partial \bar{x}^2} \mp \frac{(1-t_{\mathrm{c}}^0)}{\varepsilon_{\mathrm{e}}^{\pm} F L^{\pm}} I(t), \quad \bar{t}>0, \bar{x}\in(0^{\pm}, L^{\pm}), \tag{1}$$

$$\frac{\partial c_{\mathrm{e}}^{\pm}}{\partial \bar{x}}(\bar{t},0^{\pm}) = 0, \bar{t}\geq 0, \tag{2}$$

$$\frac{\partial c_{\mathrm{e}}^{-}}{\partial \bar{x}}(\bar{t},L^{-}) = \frac{-c_{\mathrm{e}}^{-}(\bar{t},L^{-})}{P^*}, \quad \bar{t}\geq 0, \tag{3}$$

$$\frac{\partial c_{\mathrm{e}}^{+}}{\partial \bar{x}}(\bar{t},L^{+}) = \frac{c_{\mathrm{e}}^{+}(\bar{t},L^{+})}{L^{\mathrm{sep}}-P^*}, \quad \bar{t}\geq 0, \tag{4}$$

where $\varepsilon_e^i, i\in\{-,\mathrm{sep},+\}$ denotes electrolyte phase volume fraction. t_c^0 is transference number and $L^i, i\in\{-,\mathrm{sep},+\}$ is the thickness of the battery regions. P^* is the equilibrium point, defined as $P^* = \frac{L^{\mathrm{sep}}+L^{+}-L^{-}}{2}$. The electrolyte lithium concentration in the separator $c_{\mathrm{e}}^{\mathrm{sep}}(t,x)$, and the modified boundary conditions are described as:

$$\frac{\partial c_{\mathrm{e}}^{\mathrm{sep}}}{\partial \bar{t}}(\bar{t},\bar{x}) = \frac{D_{\mathrm{e}}^{\mathrm{sep,eff}}}{\varepsilon_e^{\mathrm{sep}}}\frac{\partial^2 c_{\mathrm{e}}^{\mathrm{sep}}(\bar{t},\bar{x})}{\partial \bar{x}^2},$$

$$D_{\mathrm{e}}^{\mathrm{sep,eff}}\frac{\partial c_{\mathrm{e}}^{\mathrm{sep}}}{\partial \bar{x}}(\bar{t},0^{\mathrm{sep}}) = \frac{-c_{\mathrm{e}}^{-}(\bar{t},L^{-})}{P^*},$$

$$D_{\mathrm{e}}^{\mathrm{sep,eff}}\frac{\partial c_{\mathrm{e}}^{\mathrm{sep}}}{\partial \bar{x}}(\bar{t},L^{\mathrm{sep}}) = \frac{c_{\mathrm{e}}^{+}(\bar{t},L^{+})}{L^{\mathrm{sep}}-P^*}.$$

The initial conditions of the states represents as follows:

$$c_{\mathrm{e}}^i(0,\bar{x}) = c_{\mathrm{e},0}^i(\bar{x}), i\in\{-,\mathrm{sep},+\}.$$

Remark 1. *The electrolyte lithium concentration PDEs in the negative electrode, positive electrode, and separator have coupled boundary conditions. By considering an equilibrium point in the separator region and assuming that the electrolyte lithium concentration in the separator is quasi-linear, the boundary conditions can be decoupled [11]. To facilitate observer design, these decoupled modified boundary conditions are employed.*

III. Fault Integrated System and Fault Model

In this section, the dynamics of the electrolyte lithium concentration, incorporating the electrolyte fault, are presented, followed by the proposed distributed fault.

A. Fault integrated system

Electrolyte lithium concentration loss, a consequence of aging in lithium-ion batteries, results from degradation mechanisms such as SEI film formation and side reactions caused by the decomposition of the liquid electrolyte. This phenomenon is modeled as the added electrolyte fault $f_{\mathrm{e}}^{-}(\bar{t},\bar{x})$ to the electrolyte concentration in the negative electrode:

$$\frac{\partial c_{\mathrm{e}}^{-}}{\partial \bar{t}}(\bar{t},\bar{x}) = \frac{D_{\mathrm{e}}^{-,\mathrm{eff}}}{\varepsilon_{\mathrm{e}}^{-}}\frac{\partial^2 c_{\mathrm{e}}^{-}(\bar{t},\bar{x})}{\partial \bar{x}^2} + \frac{(1-t_{\mathrm{c}}^0)a_s^{-}}{\varepsilon_{\mathrm{e}}^{-} F L^{-}} I(\bar{t}) + f_{\mathrm{e}}^{-}(\bar{t},\bar{x}). \tag{5}$$

Remark 2. *Given the more significant SEI effect on the electrolyte lithium concentration in the negative electrode compared to the positive electrode, this work focuses on the negative electrode. This approach can be easily extended to the positive electrode.*

B. Fault function

The distributed electrolyte fault function $f_{\mathrm{e}}^{-}(\bar{t},\bar{x})$ in (5) is assumed as follows [7]:

$$f_{\mathrm{e}}^{-}(\bar{t},\bar{x}) = \theta\Omega(\bar{t}-t_{\mathrm{fau}})\beta_{\mathrm{SEI}}(\bar{x})c_{\mathrm{e}}^{-}(\bar{t},L^{-}), \tag{6}$$

where t_{fau} denotes the time at which the fault occurs in the system. The first term θ, which represents the fault's magnitude, is treated as an unknown parameter. The remaining terms, which are known terms, are considered based on the following assumption.

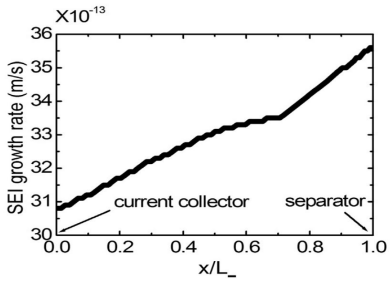

Fig. 2: Position-dependent SEI growth for Lithium Manganese Oxide battery [12].

Assumption 2 (Fault time profile)**.** *The time growth of the fault $\Omega(\tau)$, satisfies the following function [7]:*

$$\Omega(\tau) = \begin{cases} 0, & \tau<0 \\ 1-e^{-\alpha\tau}, & \tau\geq 0 \end{cases}$$

where α is constant of proportionality that comes from population growth model [13], and τ is the time at which the fault occurs in the system.

Assumption 3 (Fault growth rate)**.** *Based on the position-dependent plot of the SEI layer, as shown in Fig. 2 [12, Fig. 13], the SEI growth rate is assumed to be proportional to the spatial coordinate, defined as:*

$$\beta_{SEI}(\bar{x}) := \beta_{SEI,0^-} + \frac{\beta_{SEI,L^-}-\beta_{SEI,0^-}}{L^-}\bar{x},$$

where $\beta_{SEI,0^-} = \beta_{SEI}(0^-)$ and $\beta_{SEI,L^-} = \beta_{SEI}(L^-)$ are the SEI growth rate at the current collector/negative electrode and separator/negative electrode boundaries, respectively.

Assumption 4 (Lithium concentration effect)**.** *The electrolyte fault has a proportional relation with the lithium concentration at the electrolyte boundary $c_e^-(\bar{t}, L^-)$, similar to the modeling of electrode faults in [7].*

The growth rate at the negative electrode/separator interface is more pronounced than in other regions of the negative electrode [12]. Consequently, the lithium concentration at the L^- boundary is considered.

IV. Fault Detection Scheme

The two cascaded observer scheme for fault diagnosis is shown in Fig. 3. The first observer functions as a state

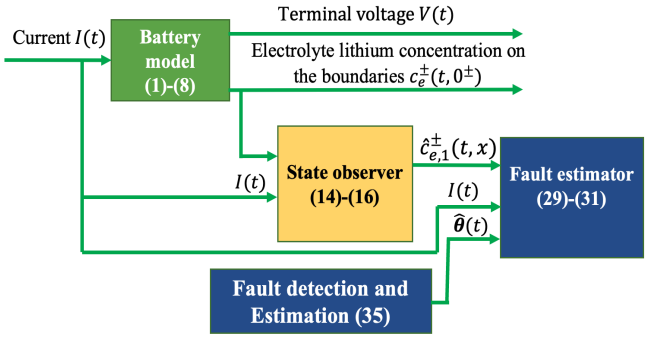

Fig. 3: Proposed observer scheme

observer, estimating the distributed electrolyte lithium concentration under both healthy and faulty conditions. The second observer, acting as a fault estimator, utilizes the state estimated by the first observer to detect and estimate electrolyte lithium concentration fault.

A. Normalized system

To facilitate the observer design, normalization is applied to (1)-(3). The spatial and temporal coordinates are scaled as $x = \frac{\bar{x}}{L^-}$ and $t = \frac{D_{\mathrm{e}}^{-,\mathrm{eff}}}{\varepsilon_{\mathrm{e}}^- (L^-)^2}\bar{t}$, respectively. The normalized lithium concentration in the electrolyte within the negative electrode, along with its normalized boundary conditions, is outlined as follows:

$$\frac{\partial c_{\mathrm{e}}^-(t,x)}{\partial t} = \frac{\partial^2 c_{\mathrm{e}}^-(t,x)}{\partial x^2} + \frac{L^-(1-t_c^0)}{D_{\mathrm{e}}^{-,\mathrm{eff}}F} I(t) + f_{\mathrm{e}}^-(t,x), t>0, x\in(0,1), \tag{7}$$

$$\frac{\partial c_{\mathrm{e}}^-}{\partial x}(t,0^-) = 0, t \geq 0, \tag{8}$$

$$\frac{\partial c_{\mathrm{e}}^-}{\partial x}(t,1^-) = \frac{-L^- c_{\mathrm{e}}^-(t,1^-)}{P^*}, t \geq 0. \tag{9}$$

B. Observer design

1) State observer: Utilizing the electrolyte concentration at the boundary $c_{\mathrm{e}}^-(t,0^-)$, the state observer is designed as follows:

$$\frac{\partial \hat{c}_{\mathrm{e},1}^-}{\partial t}(t,x) = \frac{\partial^2 \hat{c}_{\mathrm{e},1}^-}{\partial x^2}(t,x) + \frac{L^-(1-t_c^0)}{D_{\mathrm{e}}^{-,\mathrm{eff}}F} I(t) - k_1(x)(c_{\mathrm{e}}^-(t,0^-) - \hat{c}_{\mathrm{e},1}^-(t,0^-)), \tag{10}$$

$$\frac{\partial \hat{c}_{\mathrm{e},1}^-}{\partial x}(t,0^-) = k_{10}(c_{\mathrm{e},1}^-(t,0^-) - \hat{c}_{\mathrm{e},1}^-(t,0^-)), \tag{11}$$

$$\frac{\partial \hat{c}_{\mathrm{e},1}^-}{\partial x}(t,1^-) = \frac{-L^- \hat{c}_{\mathrm{e},1}^-(t,1^-)}{P^*}, \tag{12}$$

where $k_1(x)$ and k_{10} are the observer gains. The observer gains will be determined such that $\hat{c}_{\mathrm{e}}^-(t,x)$ converges to $c_{\mathrm{e}}^-(t,x)$ as time approaches infinity. State estimation error system $\tilde{c}_{\mathrm{e},1}^-(t,x) = c_{\mathrm{e}}^-(t,x) - \hat{c}_{\mathrm{e},1}^-(t,x)$ is obtained as:

$$\frac{\partial \tilde{c}_{\mathrm{e},1}^-}{\partial t}(t,x) = \frac{\partial^2 \tilde{c}_{\mathrm{e},1}^-}{\partial x^2}(t,x) + k_1(x)\tilde{c}_{\mathrm{e},1}^-(t,0^-), \tag{13}$$

$$\frac{\partial \tilde{c}_{\mathrm{e},1}^-}{\partial x}(t,0) = -k_{10}\tilde{c}_{\mathrm{e},1}^-(t,0^-), \tag{14}$$

$$\frac{\partial \tilde{c}_{\mathrm{e},1}^-}{\partial x}(t,1^-) = \frac{-L^- \tilde{c}_{\mathrm{e},1}^-(t,1^-)}{P^*}. \tag{15}$$

By applying the following invertible transformation [14]:

$$\tilde{c}_{\mathrm{e},1}^-(t,x) = \tilde{w}(t,x) - \int_0^x k(x,y)\tilde{w}(t,y)\,dy, \tag{16}$$

so that $\tilde{\omega}$ satisfies the following target system [9]:

$$\frac{\partial \tilde{w}}{\partial t}(t,x) = \frac{\partial^2 \tilde{w}}{\partial x^2}(t,x) + f_{\mathrm{e}}^-(t,x) - \gamma\tilde{w}(t,x),$$
$$\frac{\partial \tilde{w}}{\partial x}(t,0) = 0,$$
$$\frac{\partial \tilde{w}}{\partial x}(t,1^-) = -q^-\tilde{w}(t,1^-),$$

where $q^- = \frac{L^-}{P^*}$, and $\gamma \geq -\frac{1}{4}$ is a chosen parameter that determines the convergence rate of the estimated states to the system states. The gain karnel $k(x,y)$ in (16) satisfies the following PDE system:

$$\frac{\partial^2 k}{\partial x^2}(x,y) - \frac{\partial^2 k}{\partial y^2}(x,y) = -\gamma k(x,y), \tag{17}$$

$$\frac{\partial k}{\partial x}(1,y) = -q^- k(1,y), \tag{18}$$

$$k(x,x) = -\frac{\gamma}{2}x, \tag{19}$$

and the solution of the kernel function PDE (17)-(19) is achieved as follows [15]:

$$k(x,y) = \frac{-\gamma q^-}{\sqrt{\gamma + (q^-)^2}} \times \int_0^{x-y} e^{q^-\tau/2} I_0\left(\sqrt{\gamma(2-x-y)(x-y-\tau)}\right) \times \sinh\left(\frac{\sqrt{\gamma+(q^-)^2}}{2}\tau\right) d\tau - \gamma(1-y)\frac{I_1\left(\sqrt{\gamma\left((1-y)^2-(1-x)^2\right)}\right)}{\sqrt{\gamma\left((1-y)^2-(1-x)^2\right)}},$$

where $I_m(\cdot)$ is the modified Bessel function of the first kind, and m denotes the order of the Bessel function [14, Appendix A.2]. The observer gains $k_1(x)$ and k_{10} are determined to ensure the stability of the estimation error system (13)-(15) by solving the kernel function, and are obtained as follows:

$$k_1(x) = -k_y(x,0),$$
$$k_{10} = -\frac{\gamma}{2}.$$

Remark 3. *Note that the lithium electrolyte concentration at the boundaries can be determined by measuring related parameters, such as electrolyte resistance at the boundaries, using Electrochemical Impedance Spectroscopy (EIS), as thoroughly discussed in [16].*

Theorem 1. *Consider the error dynamics* (13)-(15)*. Under assumptions 1-4 for any initial condition, if* $\gamma \geq -\frac{1}{4}$*, due to the invertibility of the transformation* (16)*:*
1) In the absence of fault ($f_e^-(t,x) = 0, \forall (t,x) \in [0,\infty] \times [0,1^-]$*), the estimation error is exponentially stable in the sense of the spatial* $\mathcal{L}_2$ *norm.*
2) In the presence of fault ($f_e^-(t,x) \neq 0, \exists (t,x), t \in [0,\infty] \times [0,1^-]$*), the estimation error remains bounded.*

Proof. Detailed proofs for both cases are provided in [9], with $\Delta_\omega Q(t,x)$ replaced by $f_{\text{e}}^-(t,x)$. □

2) Fault estimator: Using the estimated lithium electrolyte concentration distribution $\hat{c}_{\text{e},1}^-(t,x)$, produced by the state observer, the fault estimator is proposed as follows:

$$\frac{\partial \hat{c}_{\text{e},2}^-}{\partial t}(t,x) = \frac{\partial^2 \hat{c}_{\text{e},2}^-}{\partial x^2}(t,x) + \frac{L^-(1-t_c^0)}{D_{\text{e}}^{-,\text{eff}} F} I(t) + \hat{\theta}(t)\psi(t,x) + k_2\left(\hat{c}_{\text{e},1}^-(t,x) - \hat{c}_{\text{e},2}^-(t,x)\right), \tag{20}$$

$$\frac{\partial \hat{c}_{\text{e},2}^-}{\partial x}(t,0^-) = k_{10}\tilde{c}_{\text{e},1}^-(t,0^-) - \frac{1}{2}\tilde{c}_{\text{e},3}^-(t,0^-), \tag{21}$$

$$\frac{\partial \hat{c}_{\text{e},2}^-}{\partial x}(t,1^-) = \frac{-L^-\hat{c}_{\text{e},1}^-(t,1^-)}{P^*}, \tag{22}$$

where $\psi(t,x) = \Omega(t - t_{\text{fau}})\beta_{\text{SEI}}(x)c_{\text{e}}^-(t,1^-)$ is the known term of fault. The observer gain k_2 will be determined later in such a way that it guarantees the stability of the estimation error $\tilde{c}_{\text{e},2}^-(t,x) = c_{\text{e}}^-(t,x) - \hat{c}_{\text{e},2}^-(t,x)$, for which the system is given by:

$$\frac{\partial \tilde{c}_{\text{e},2}^-}{\partial t}(t,x) = \frac{\partial^2 \tilde{c}_{\text{e},2}^-}{\partial x^2}(t,x) - \tilde{\theta}(t)\psi(t,x) - k_2\left(\hat{c}_{\text{e},1}^-(t,x) - \hat{c}_{\text{e},2}^-(t,x)\right),$$
$$\frac{\partial \tilde{c}_{\text{e},2}^-}{\partial x}(t,0^-) = -k_{10}\tilde{c}_{\text{e},1}^-(t,0^-),$$
$$\frac{\partial \tilde{c}_{\text{e},2}^-}{\partial x}(t,1^-) = \frac{-L^-\tilde{c}_{\text{e},1}^-(t,1^-)}{P^*},$$

where $\tilde{\theta}(t) = \theta - \hat{\theta}(t)$. The function $\tilde{\theta}(t)$ is chosen to satisfy the following update law:

$$\dot{\hat{\theta}}(t) = \frac{1}{k_3}\int_0^1 \psi(t,x)\tilde{c}_{\text{e},3}(t,x)\,dx - \hat{\theta}(t)\left\|\tilde{c}_{\text{e},3}(t,\cdot)\right\|, \tag{23}$$

where $\tilde{c}_{\text{e},3}^-(t,x) = \hat{c}_{\text{e},1}^-(t,x) - \hat{c}_{\text{e},2}^-(t,x)$ and $k_3 > 0$ is a selected gain that regulates the rate at which the parameter converges, and $\|\cdot\|$ denotes the $\mathcal{L}_2$-norm.

The threshold level, denoted by ϵ, is considered non-zero to account for the uncertainty effect, as defined by the probability of false alarm approach [9]. the system is considered fault-free when the residual signal remains below or equal to the threshold, i.e., $\hat{\theta}(t) \leq \epsilon$ and fault is detected when the residual signal exceeds threshold $\hat{\theta}(t) > \epsilon$. Note that in this study, the residual signal is defined as the state estimation error and is used for fault detection when it exceeds a threshold level.

Theorem 2. *Consider the electrolyte lithium concentration in* (7)-(9) *and the proposed observer* (20)-(22) *with the update law in* (23)*. If* $k_2 < 1/4$ *and* $k_3 > 0$*, then for any initial conditions under the given assumptions 1-4, the distributed state estimation error* $\tilde{c}_{e,2}^-(t,x)$ *and the parameter estimation error* $\tilde{\theta}(t)$ *are uniformly ultimately bounded under conditions* (24) *and* (25) *with the ultimate bound given in* (26)*.*

Proof. Consider the following Lyapunov function candidate:

$$W_2(t) = \frac{1}{2}\left\|\tilde{c}_{\text{e},3}^-(t,\cdot)\right\|^2 + \frac{k_3}{2}\tilde{\theta}(t)^2.$$

By taking its time derivative and applying integration by parts and the Poincaré inequality [14, Lemma 2.1], one can obtain:

$$\dot{W}_2(t) \leq \int_0^1 \|\tilde{c}_{\text{e},3}(t,\cdot)\|\left(-\left(\frac{1}{4} - k_2\right)\|\tilde{c}_{\text{e},3}(t,\cdot)\| - \xi\delta - \psi_{\max}\theta_{\max} + k_3\left(\left|\tilde{\theta}(t)\right| - \frac{1}{2}\theta_{\max}\right)^2 + \frac{k_3}{4}\theta_{\max}\right)dx,$$

where $\xi := \max_{x\in[0,1]} k_1(x)$, and $\delta := \sup_{t\in[0,\infty]} \tilde{c}_{\text{e},1}(t,0^-)$.

Define $\boldsymbol{h}(t) = \left[\left\|\tilde{c}_{\text{e},3}^-(t,\cdot)\right\| \quad \tilde{\theta}(t)\right]$, it can be concluded that:

$$\min\{1,k_3\}\|\boldsymbol{h}(t)\|^2 \leqslant W_2(t) \leqslant \max\{1,k_3\}\|\boldsymbol{h}(t)\|^2.$$

By considering $\alpha_1(r) = \min\{1,k_3\}r^2$ and $\alpha_2(r) = \max\{1,k_3\}r^2$, based on [17, Section 4.8], if $k_2 < \frac{1}{4}$, under one of the following conditions:

$$\|\tilde{c}_{\text{e},3}(t,\cdot)\| \geq \frac{\delta\xi + \psi_{\max}\theta_{\max} + \frac{k_3}{4}\theta_{\max}}{\frac{1}{4} - k_2} := \mu_1, \tag{24}$$

$$\left|\tilde{\theta}(t)\right| \geq \sqrt{\frac{\delta\xi + \psi_{\max}\theta_{\max} + \frac{k_3}{4}\theta_{\max}^2}{k_3}} + \frac{\theta_{\max}}{2} := \mu_2, \tag{25}$$

the estimation error $\boldsymbol{h(t)}$ is uniformly ultimately bounded. Indeed, define

$$\mu = \left|\begin{bmatrix}\mu_1 & \mu_2\end{bmatrix}\right|,$$

where $|\cdot|$ denotes 2-norm, then based on [17, Section 4.8], for every initial states $\boldsymbol{h}(0)$, satisfying $\|\boldsymbol{h}(0)\| \leq \alpha_2^{-1}(\alpha_1(r))$,

there is $T \geq 0$ (dependent of $\boldsymbol{h}(0)$ and μ) such that [17, Section 4.8]:

$$\|\boldsymbol{h}(\boldsymbol{t})\| \leq b = \alpha_1^{-1}(\alpha_2(\mu)) = \sqrt{\frac{\max\{1, k_3\}}{\min\{1, k_3\}}}\mu, \forall t \geq T. \tag{26}$$

□

From (24), increasing k_2 increases the ultimate bound by influencing μ. Based on (26), it can be concluded that:

- **Case 1:** If $0 < k_3 \leq 1$, then $b = \mu\sqrt{\frac{1}{k_3}}$. Thus, increasing k_3 will reduce the ultimate bound.
- **Case 2:** If $k_3 > 1$, then $b = \mu\sqrt{k_3}$. Thus, decreasing k_3 will reduce the ultimate bound.

Therefore, we choose $k_3 = 1$.

V. Simulation

The simulation is conducted on a $LiFePO_4$ battery cell with the parameters referenced from Table 1 in [18]. The temperature is kept constant at $T = 298$ K. The UDDS input current profile [19] is depicted in Fig. 4. The estimation error

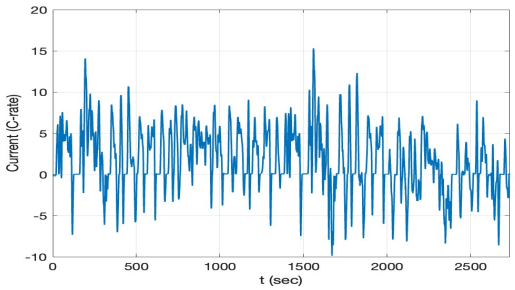

Fig. 4: UDDS current profile

$\tilde{c}_{e,1}^{-}(t,x)$ of the state observer (10)-(12) is plotted in Fig. 5. The initial conditions for the original system and the observer are selected to be different to ensure the convergence of the design. The fault function for the simulation is defined as

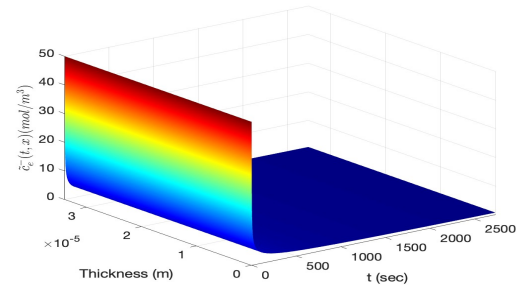

Fig. 5: Estimation error $\tilde{c}_{e,1}^{-}(t,x)$ in the absence of fault

follows:

$$f_e(t,x) = 50(1 - e^{-0.0001(t-1000)})c_e^{-}(t,1^{-}) \times \left(\beta_{SEI}(0^{-}) + \left(\beta_{SEI}(1^{-}) - \beta_{SEI}(0^{-})\right)x\right), \tag{27}$$

where $\beta_{SEI}(0^{-}) = 31 \times 10^{-13}$ and $\beta_{SEI}(1^{-}) = 36 \times 10^{-13}$ [12]. The distributed fault, injected into the system at $t_{fau} =$

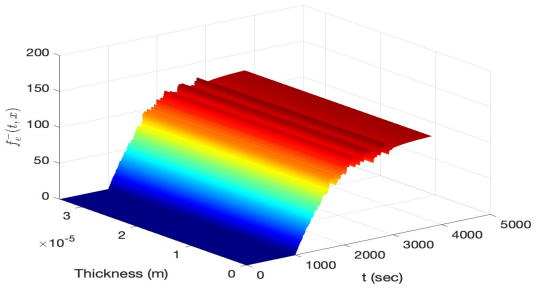

Fig. 6: Distributed fault $f_e^{-}(t,x)$.

1000 s, is illustrated in Fig. 6. As t increases, the second term of (27), $1 - e^{-0.0001(t-1000)}$, which represents the fault time profile, approaches 1. The last term remains small due to the slow growth rate and minimal thickness of the SEI layer. Therefore, the dominant component of the fault will be $c_e^{-}(t,1^{-})$. This dominant effect is evident in Fig. 6, where, after the occurrence of the fault in the system at $t_{fau} \geq 1000$ s, the fault behavior closely resembles the system state. In the presence of the fault, the estimated state is shown in Fig. 7. After the fault is injected, the lithium concentration

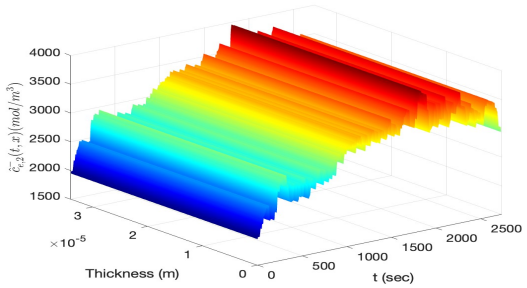

Fig. 7: Estimated electrolyte lithium concentration in the negative electrode $\hat{c}_{e,2}^{-}(t,x)$ in the presence of fault

increases, as illustrated in Fig. 8. The estimation error in

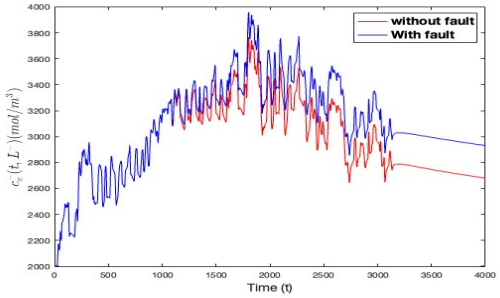

Fig. 8: Comparison of true electrolyte lithium concentration $c_{e,2}^{-}(t,1^{-})$ in the presence and absence of fault

the presence of fault is illustrated in Fig. 9, demonstrating that the designed observer can efficiently detect the fault. In Fig. 10, the fault estimation at the boundary is depicted. Threshold level is set on $\epsilon = 15$ and the fault is detected after about 80 seconds. Once the threshold is exceeded, the fault is detected, and the fault magnitude is accurately estimated

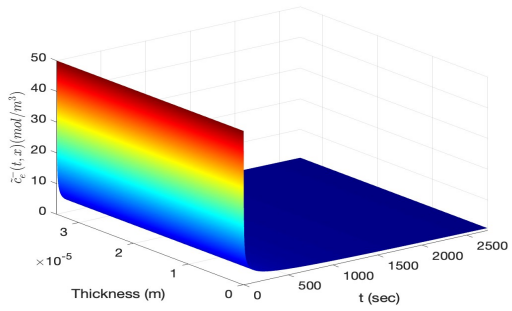

Fig. 9: Estimation error $\tilde{c}_{e,2}^-(t,x)$ in the presence of fault

as shown in 10.

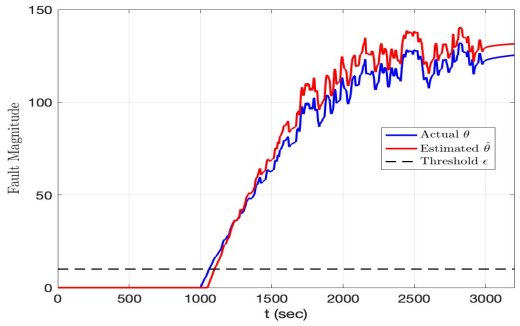

Fig. 10: Fault detection and estimation

VI. Conclusion and Future Work

In this study, a model-based fault detection and estimation scheme for electrolyte lithium concentration degradation in lithium-ion batteries is proposed. The fault detection system consists of two cascaded PDE observers: the state observer and the fault estimator. The electrolyte fault is a physically relevant function characterized by an unknown magnitude, which can be estimated using the designed update law. The effectiveness of the proposed scheme was validated through the simulations. Future work will focus on applying this fault estimation to obtain the remaining useful life of the battery. Additionally, it aims to conduct experimental validations to assess the scheme's performance under practical conditions while considering potential parameter uncertainties, particularly those related to electrolyte dynamics, which are challenging to estimate accurately.

Acknowledgments

The authors would like to acknowledge Professor Satadru Dey for his comments on electrochemical fault modeling.

References

[1] Vahid Safavi, Arash Mohammadi Vaniar, Najmeh Bazmohammadi, Juan C Vasquez, Ozan Keysan, and Josep M Guerrero. A battery degradation-aware energy management system for agricultural microgrids. *Journal of Energy Storage*, 108:115059, 2025.

[2] Ferran Brosa Planella and W Dhammika Widanage. A single particle model with electrolyte and side reactions for degradation of lithium-ion batteries. *Applied Mathematical Modelling*, 121:586–610, 2023.

[3] Weixiong Wu, Wei Wu, Xianghui Qiu, and Shuangfeng Wang. Low-temperature reversible capacity loss and aging mechanism in lithium-ion batteries for different discharge profiles. *International journal of energy research*, 43(1):243–253, 2019.

[4] Xiaosong Hu, Kai Zhang, Kailong Liu, Xianke Lin, Satadru Dey, and Simona Onori. Advanced fault diagnosis for lithium-ion battery systems: A review of fault mechanisms, fault features, and diagnosis procedures. *IEEE Industrial Electronics Magazine*, 14(3):65–91, 2020.

[5] Chengzhong Zhang, Hongyu Zhao, Lifang Wang, and Chenglin Liao. Lithium-ion batteries early internal short-circuit fault quantitative identification during charging and setting periods. *IEEE Transactions on Industrial Electronics*, 2025.

[6] Shanthan Kumar Padisala, Sara Sattarzadeh, and Satadru Dey. Reduced and reformulated electrochemical model-based detection and isolation of electrode-level faults in lithium-ion battery cells. *IFAC-PapersOnLine*, 55(37):734–739, 2022.

[7] Hasan Ferdowsi and Sarangapani Jagannathan. Fault diagnosis of a class of distributed parameter systems modeled by parabolic partial differential equations. In *American Control Conference*, pages 5434–5439. IEEE, 2014.

[8] Satadru Dey and Beshah Ayalew. A diagnostic scheme for detection, isolation and estimation of electrochemical faults in lithium-ion cells. In *Dynamic Systems and Control Conference*, volume 57243, page V001T13A001. American Society of Mechanical Engineers, 2015.

[9] Satadru Dey, Hector E Perez, and Scott J Moura. Model-based battery thermal fault diagnostics: Algorithms, analysis, and experiments. *IEEE Transactions on Control Systems Technology*, 27(2):576–587, 2017.

[10] Jianing Xu, Tiansi Wang, Lei Pei, Shitong Mao, and Chunbo Zhu. Parameter identification of electrolyte decomposition state in lithium-ion batteries based on a reduced pseudo two-dimensional model with Padé approximation. *Journal of Power Sources*, 460:228093, 2020.

[11] Sara Sepasiahooyi and Shu-Xia Tang. Enhanced battery state estimation: Part 1 - electrolyte lithium-ion concentration observer. In *2024 IEEE 63rd Conference on Decision and Control (CDC)*, pages 3422–3427, 2024.

[12] Lin Liu, Jonghyun Park, Xianke Lin, Ann Marie Sastry, and Wei Lu. A thermal-electrochemical model that gives spatial-dependent growth of solid electrolyte interphase in a li-ion battery. *Journal of power sources*, 268:482–490, 2014.

[13] Basel M Al-Eideh and Hana O Al-Omar. Population projection model using exponential growth function with a birth and death diffusion growth rate processes. *Eur. J. Sci. Res*, 151(3):271–276, 2019.

[14] Miroslav Krstic and Andrey Smyshlyaev. *Boundary control of PDEs: A course on backstepping designs*. SIAM, 2008.

[15] Bhathiya Rathnayake, Mamadou Diagne, Nicolás Espitia, and Iasson Karafyllis. Observer-based event-triggered boundary control of a class of reaction–diffusion pdes. *IEEE Transactions on Automatic Control*, 67(6):2905–2917, 2021.

[16] Sara Sepasiahooyi and Shu-Xia Tang. Enhanced battery state estimation: Part 2 - reverse sensitivity analysis and electrode lithium-ion observer. In *2024 IEEE 63rd Conference on Decision and Control (CDC)*, pages 4251–4256, 2024.

[17] Hassan K. Khalil. *Nonlinear Systems*. Prentice Hall, Upper Saddle River, NJ, 3rd edition, 2002.

[18] Clément Edouard, Martin Petit, C Forgez, Julien Bernard, and Renaud Revel. Parameter sensitivity analysis of a simplified electrochemical and thermal model for li-ion batteries aging. *Journal of Power Sources*, 325:482–494, 2016.

[19] Scott J Moura, Federico Bribiesca Argomedo, Reinhardt Klein, Anahita Mirtabatabaei, and Miroslav Krstic. Battery state estimation for a single particle model with electrolyte dynamics. *IEEE Transactions on Control Systems Technology*, 25(2):453–468, 2016.